Solid Freeform Fabrication 2021: Proceedings of the 32nd Annual International Solid Freeform Fabrication Symposium – An Additive Manufacturing Conference
Reviewed Paper

THE ANISOTROPIC YIELD SURFACE OF CELLULAR MATERIALS

Kaitlynn M Conway*; Zachary Romanick*; Lea M Cook*; Luis A Morales*; Jonathan D Despeaux*; Marcus L Ridlehuber*; Christian Fingar*; Daquan Doctor*; Garrett J Pataky*
*Department of Mechanical Engineering, Clemson University, Clemson, SC 29631

Abstract

Mechanical metamaterials are often limited in engineering applications because of uncertainty in their deformation behavior. This uncertainty necessitates large factors of safety and behavior assumptions to be included in mechanical metamaterial designs, detracting from the largest benefit of metamaterials: their ultralight weight. In this study, a yield envelope was created for both a bending dominated and a stretching dominated cellular material topology to improve the understanding of the response of cellular materials under various load types and orientations. Experimental studies revealed that the shear strength of a cellular material is significantly less than that predicted by the Mohr's criterion, necessitating a modification of the Mohr's yield criterion for cellular materials. Both topologies experienced tension-compression anisotropy and anisotropy dependent on the topology orientation during loading with the stretching dominated topology experiencing the largest anisotropies.

A substantially improved version of this paper appears in a special issue of the TMS publication *JOM*, March 2022.

Introduction

Monolithic materials, in terms of specific strength, are limited by their elemental weights creating a ceiling of what can be achieved via solid materials alone. An increasingly popular method for manipulating a material's properties, is through the geometric arrangement or topology of the material's mesostructure [1]. Low density metamaterials combine solid materials and zero density voids to occupy material property spaces not achievable by monolithic materials [2]. The complex geometric freedoms additive manufacturing (AM) affords enables for the creation of metamaterial topologies with significantly altered mechanical properties compared to the base materials [3]. However, understanding of the mechanics responsible for these metamaterial's deformation behavior, particularly fracture and failure, across different environments and loading situations is understudied, necessitating large factors of safety [1]. This conservative approach detracts from the largest benefit of metamaterials: their ultralight weight.

Low-density metamaterials have evolved from honeycomb sandwich boards [4] and disordered foams [5] to highly complex topologies across a variety of size scales and base materials [1]. The rapid advances in metamaterial use and design has resulted in the introduction of new topologies to the scientific community, outpacing the understanding of failure mechanisms. Additionally, there is not a consistency among studies of base material, cell size, or AM process which makes comparing

various topologies across reported studies difficult at best and speculative at worst. Mechanical metamaterials are known to have tension and compression asymmetry [6] as well as orientation-dependent anisotropic behavior when loading due to lack of rotational symmetry of many topologies [7]. Additional studies of metamaterials have found the shear strength of metamaterials to be significantly less than that of the uniaxial strength [8]. Due to this, metamaterials will have a complex, non-trivial yield envelope that is crucial for engineers to understand to design metamaterial components with confidence.

The goal of this study was to determine the effect of topology, particularly stretching and bending dominated topologies, on the yield surface size and shape. Mohr's criterion was chosen for this study as it was designed to handle tension-compression anisotropy and the failure envelope can be determined with three tests: tension, compression, and pure shear [9].

Methods and Materials

Four cellular metamaterial topologies of interest were AM by fused deposition modeling: a traditional honeycomb, an auxetic honeycomb, a triangular, and a circular topology. Topologies were modeled with a 5 mm unit cell and a 0.6 mm wall thickness and were printed on a Dremel 3D45 printer using Dremel Eco-ABS white filament [10]. Each topology was tested in two orientations, deemed σ_1 and σ_2, where σ_2 is a 90° in plane rotation of σ_1, Figure 1.

Specimens of all four topologies were tested in tension, compression, and shear to populate the Mohr's Circle. Three specimens of each type were tested in each loading condition and the yield strengths calculated by a 0.2% offset were averaged. Novel pure shear grips previously designed by the authors were used to insure pure shear rather than a combined shear and uniaxial loading state [8].

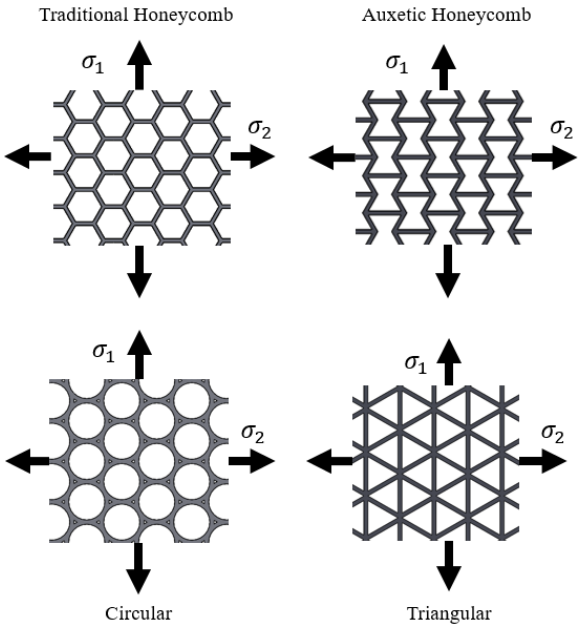

Figure 1: Cellular material topologies tested with original orientation (σ_1) and 90° rotation (σ_2)

Experiments were performed in displacement control at a rate of 30 μm/s using a hydraulic load frame for the shear specimens and a screw-driven load frame for the tension and compression samples. A single camera captured a 6-by-4 unit cell cross section of the center of each specimen during tests and digital image correlation was used to calculate the strains in the cellular material during deformation. The camera used was a Point Grey model GS3 equipped with a Navitar lens and a 1X adaptor and captured images at a rate of 1 Hz. Images were used to calculate the full field displacement and strains using commercial digital image correlation software, VIC 2D. Strain calculations were performed with a virtual strain gage of 21 pixels^2 and a spatial resolution of 35 pixels^2 following the procedure outlined in [11]. Global material properties were calculated using the area methodology outlined in [7].

Results

Shear Strength

Experimentally determined tension, compression, and shear yield stresses for each orientation of the chosen topologies were plotted as a Mohr's circle, shown for the honeycomb topology in Figure 2a,b. The max shear line is calculated by plotting a linear line between the maximum shear value of each Mohr's circle. The max shear line is displayed in green in Figure 2a,b. The max shear line was selected rather than a tangential line to the Mohr's circles offering a more conservative yield envelope. As cellular materials are sensitive to defects from the AM process, a conservative yield criterion was preferable. Using the max shear line failure envelope, a yield surface was created for the σ_1 and σ_2 orientations, shown in Figure 2c [9]. The two yield surfaces were collapsed to one surface for the material using all six experimentally determined yield strengths to create a surface showing the full tension-compression-shear anisotropy as well as the orientation specific anisotropy, Figure 2d. The yield surfaces for each orientation are shown in Figure 3, where the top row is the yield surface for each orientation, the middle row is the combined yield surface, and the bottom row is an image of the corresponding topology.

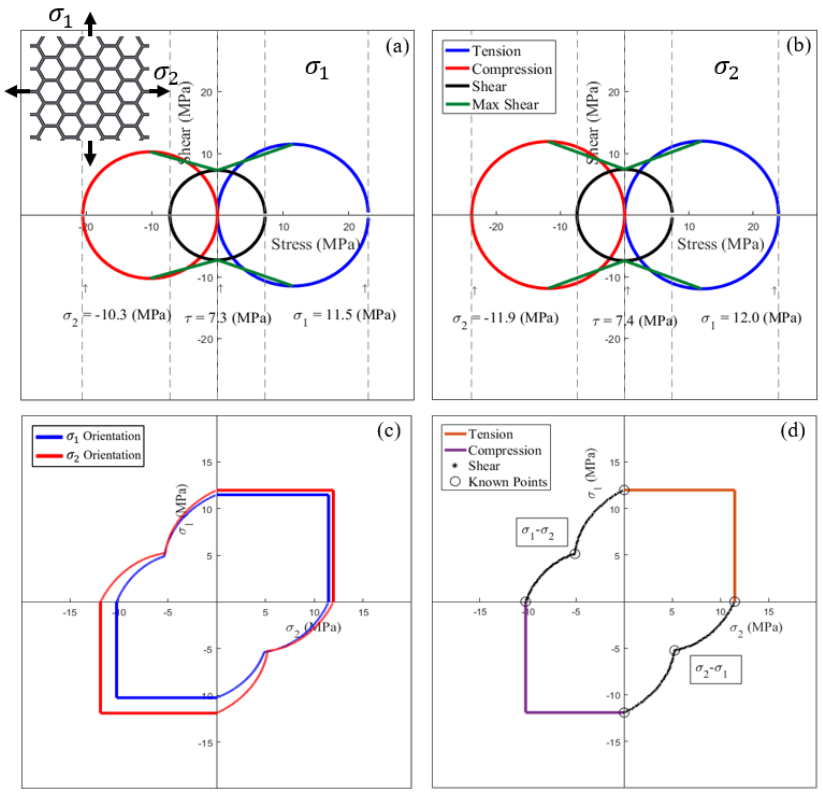

Figure 2: Honeycomb Mohr's Circle and Yield Surface

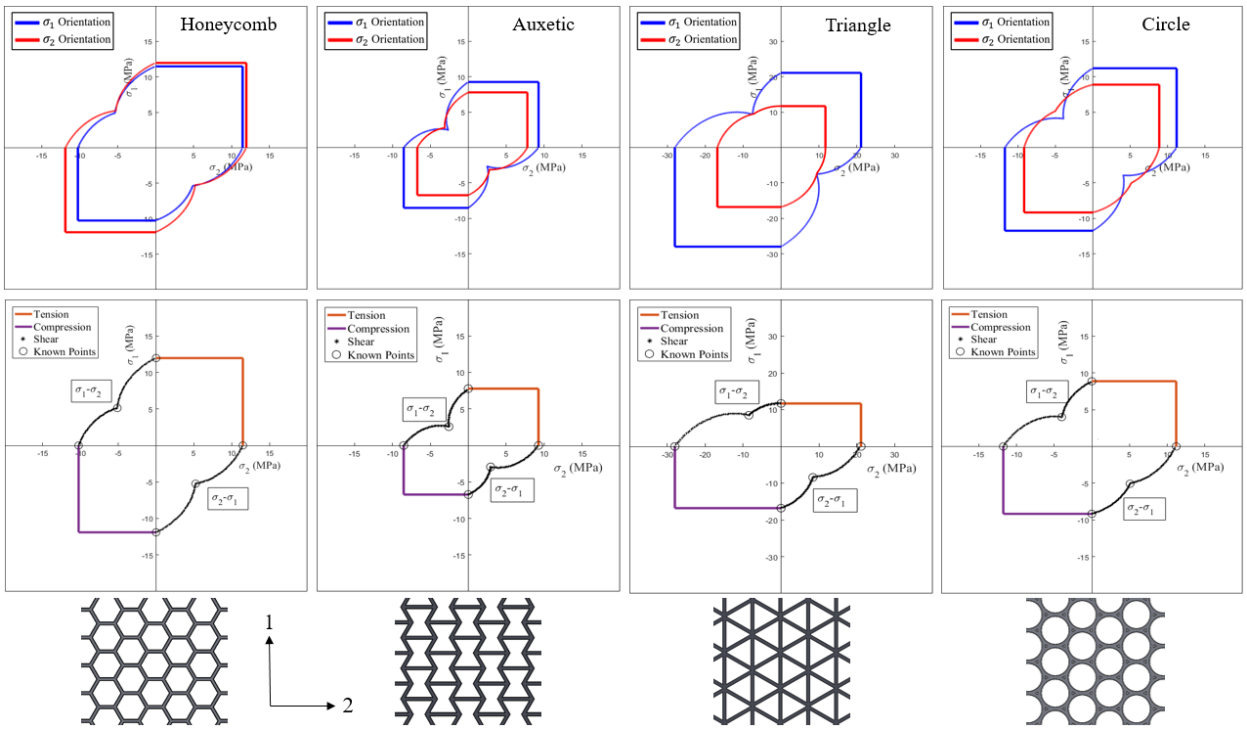

Figure 3: Yield Surface for selected topologies. Top row: Yield surface for each orientation. Middle row: Full field surface for topology. Bottom row: Selected topology. Scale adjusted for the triangle orientation

The decreased shear strength of these cellular materials resulted in a discontinuity at the pure shear loading condition. The metamaterial was weaker in shear than would be expected from the maximum-distortion-energy theory or the more conservative maximum-shear-stress theory [12]. This behavior was seen in every topology.

The stretching and bending topologies have a topology-driven strength-ductility trade off, Figure 4a. Stretching dominated topologies were stronger, while bending topologies were more ductile. This has been well-documented in metamaterial research [13–16]. In the stretching dominated triangle topology, there is a high concentration of strain very localized at the strut junctions, even at low global displacements. These strains are circled in red in Figure 4b, taken at 0.5 σ_{yield}. With further loading, the triangle topology yields and then catastrophically fails when a crack develops at one of the highlighted junctions. In the bending dominated topologies, the honeycomb and auxetic unit cells in Figure 4c and Figure 4d respectively, as the metamaterial is loaded, stress is primarily concentrated in the vertically aligned struts. This concentration of stress causes localized buckling of a strut, circled in red in Figure 4c. When a strut buckles, the stresses on the neighboring struts increase and the neighboring struts buckle as well creating a row-by-row collapse of the metamaterial. Figure 4c,d were taken immediately after yield to illustrate the buckling cell wall.

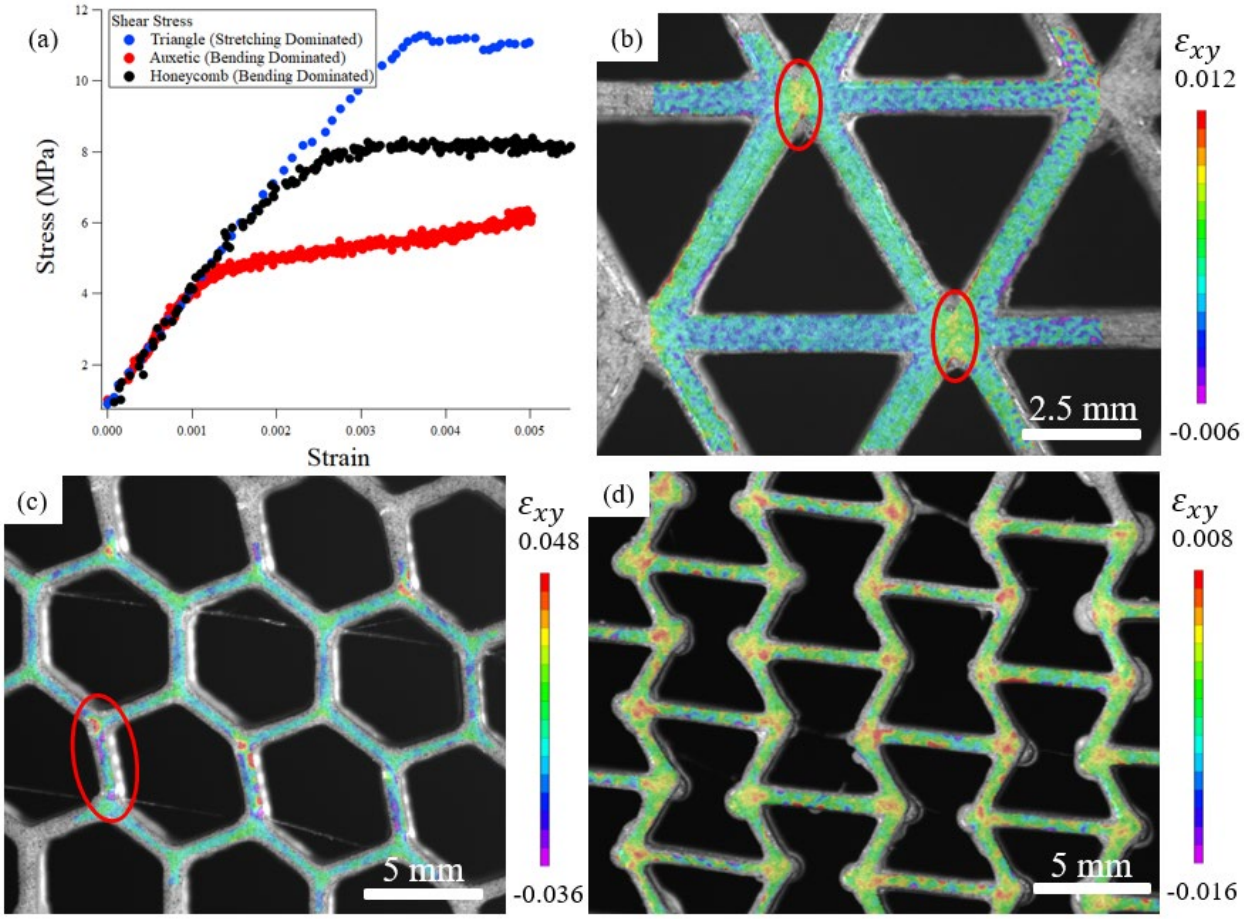

Figure 4: a) Shear stress-strain curves of selected topologies b) Strain maps of triangle in shear c) Strain maps of honeycomb in shear d) Strain map of auxetic in shear

Topology Effects

The stretching dominated triangle topology has the largest yield surface with a maximum tensile, compressive, and shear strength of 21.1 MPa, -28 MPa, and 12 MPa, respectively, over the honeycomb topology, which had the second largest yield surface, with a maximum tension, compressive, and shear strength of 12 MPa, -11.9 MPa, and 7.4 MPa, respectively. The triangle topology has a different scale than the other topologies in Figure 3 due to the greater strength. The increased strength of the honeycomb topology in comparison to other bending dominated topologies is due to the uniform deformation of the honeycomb unit cells during loading and the uniform formation of plastic hinges at the sharp corners, circled in red in Figure 5a. As the honeycomb is deformed, plastic hinges form as the arms rotate, absorbing energy and increasing the toughness. Uniform deformation allows the plastic hinges to develop without the stress concentration at any one plastic hinge becoming so large the metamaterial prematurely fractures. Figure 5 is shown after yielding to better illuminate the locations of strain and plastic hinges within the topologies, but the onset of crazing at plastic hinges has been shown to occur prior to yielding [7,18]. The circle topology does not have sharp corners for plastic hinges to form. Additionally, the hourglass shape of each strut creates a local stress concentration in the middle of the length of the strut identified by the high strain circled in red in Figure 5b. With increased loading, the local stress concentration increases leading to early fracture of individual struts lowering the yield stress, creating a smaller yield surface than the honeycomb topology. The auxetic honeycomb also develops plastic hinges when loaded; however, the auxetic honeycomb has a negative Poison's ratio [19]. As the auxetic honeycomb is loaded in tension, the horizontal struts are loaded in compression due to the negative Poison's ratio (the struts in the honeycomb topology are loaded in tension). The auxetic unit cells rotate when loaded to decrease the compressive stress on the horizontal strut, changing the loading path and non-uniformly increasing the stress concentrations at the plastic hinges. The auxetic specimen yields when the plastic hinges with the largest strain concentrations, such as that circled in Figure 5c, fracture.

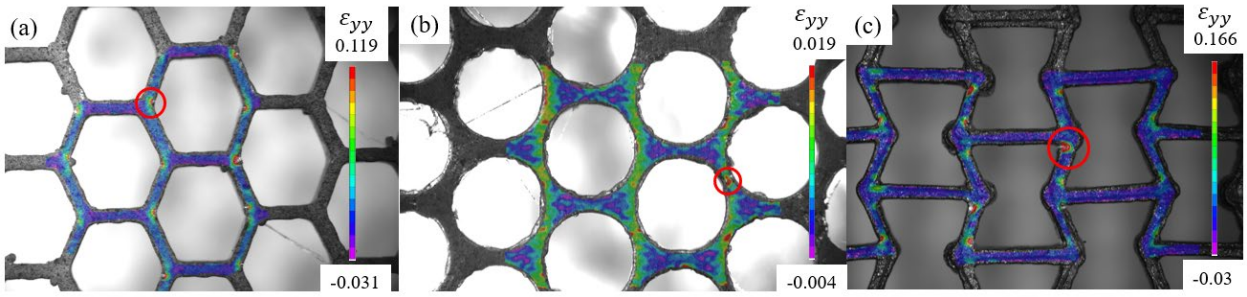

Figure 5: Strain maps of topologies in the σ_1 orientation under tensile loading, all figures the same scale

Topological-Induced Anisotropy

The triangle topology had the largest orientation anisotropy with an 80% change in tensile strength and a 66% change in compressive strength from loading in the σ_1 orientation to the σ_2 orientation. The circle topology had the next largest orientation anisotropy with 25% tensile and 27% compressive difference in strength. When the triangle topology is loaded in the σ_1 direction the axial load is primarily distributed among a third of the struts, the struts parallel to the

direction of loading. The positive axial load path is marked in red in Figure 6a and supported by the concentration of positive strains along these struts shown in Figure 6c. When loaded in the σ_2 direction, the axial load is distributed among the angled struts, Figure 6b, consisting of two thirds of the struts in the topology as demonstrated by the positive strains in Figure 6d. This difference in load distribution between the orientations explains why the tension and compression yield strength of the σ_2 orientation is nearly twice the tension and compression yield strength of the σ_1 orientation.

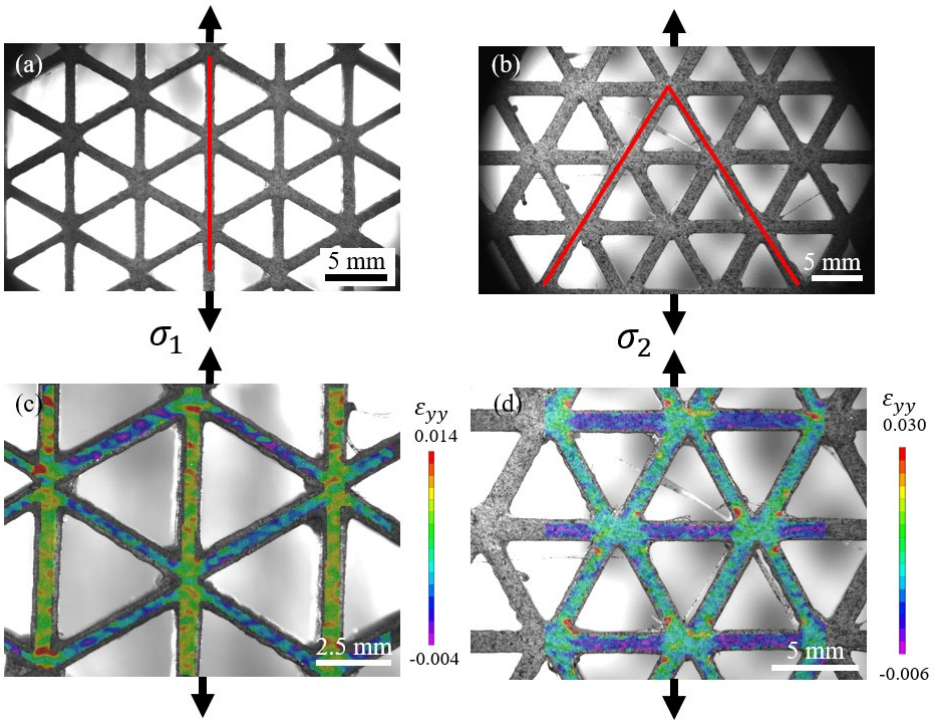

Figure 6: Axial load in a stretching dominated topology is distributed along the struts parallel to the loading direction, in the triangle topology in the σ_1 orientation the axial load is distributed primarily amongst a third of the struts, in the σ_2 orientation the axial load is distributed amongst two thirds of the struts

Discussion

There is a debate about whether to treat a mechanical metamaterial as a continuous material and use a homogenization analysis [20] or a structure and analyze the behavior using the local behavior driven by the unit cell topology [21]. Both approaches have merit and are particularly useful in specific applications. During elastic deformation, the homogenization approach of considering the metamaterial as a uniform material simplifies identifying global material properties, regardless of local plasticity that is occurring before fracture. However, identification of local stress and strain accumulation within the unit cell throughout loading is essential for understanding and predicting differences in the plastic and fracture behavior between topologies. Some studies have incorporated a two scale approach to incorporate both methodologies when analyzing

metamaterials to use the local behavior of the lattice to determine the global behavior of the material while limiting the computational work required to analyze an entire lattice structure [14,22]. In this study, a global evaluation of the metamaterial was used to calculate the yield strength of the selected topologies; however, analysis of local strain concentrations within the unit cells were investigated to explain the change in yield surface shapes between topologies. Local analysis of the lattice was not limited to a single unit cell but rather the 6-by-4 unit cell cross section captured by the camera where digital image correlation was performed. This consideration of several unit cells rather than a single cell allowed for evaluation of uniformity and the measurement of unbalanced local deformation such as the rotation and uneven plastic hinges in the auxetic topology. Evaluation of stress concentrations and local deformations within the lattice unit cells were then connected to the metamaterial yield surface size and shape to analyze how topology drives the yield surface.

The poor shear strength of cellular materials creates a yield surface shape that would not be expected from a monolithic material due to the formation of local plastic hinges and strains non-uniformly distributed among the metamaterial's struts. Yielding of the metamaterial is caused by buckling of a cell wall or fracture of a cell wall or joint on the mesoscopic scale rather than at the microstructural level as would occur with a monolithic material. This departure from traditional mechanisms of yielding in a material is shown by discontinuities on the yield surface that occur at the pure shear loading. The large variation in the size of the yield surface of the tested metamaterials further supports the need to consider metamaterials, at least partially, as a structure. All topologies in this study were produced using the same filament material, yet the maximum compressive strength of the triangle topology was over three times that of the auxetic topology and twice the honeycomb topology. Additionally, the extreme strength anisotropy between was amplified beyond a tensile-compressive strength differential, but also orientation dependence due to changing loading paths. This behavior is more typical of a structure than a conventional material.

Conclusion

A yield surface was created for four cellular material topologies tested in tension, compression, and shear. The yield surfaces demonstrated cellular materials were weakest in shear loading and have large anisotropies dependent on loading condition and orientation. Local strain fields were used to identify the mechanisms driving the deformation of different topologies and the driving effect of the unit cell deformation mechanism on global plastic properties. Buckling of cell walls and the formation of plastic hinges were the main mechanisms to cause yielding within the materials; however, rotation of the cell walls due to its negative Poison's ratio caused the auxetic topology to have the smallest yield surface.

Acknowledgements

The authors would like to thank Student Pathways in Engineering and Computing for Transfer Success, NSF Grant 1834081, at Clemson University for support of this research.

References

[1] X. Yu, J. Zhou, H. Liang, Z. Jiang, L. Wu, Mechanical metamaterials associated with stiffness, rigidity and compressibility: A brief review, Prog. Mater. Sci. 94 (2018) 114–173. doi:10.1016/j.pmatsci.2017.12.003.

[2] J.U. Surjadi, L. Gao, H. Du, X. Li, X. Xiong, N.X. Fang, Y. Lu, Mechanical metamaterials and their engineering applications, Adv. Eng. Mater. 21 (2019) 1–37. doi:10.1002/adem.201800864.

[3] O. Al-Ketan, R.K. Abu Al-Rub, Multifunctional mechanical metamaterials based on triply periodic minimal surface lattices, Adv. Eng. Mater. 21 (2019) 1–39. doi:10.1002/adem.201900524.

[4] A. Petras, M.P.F. Sutcliffe, M.P.F.S. A. Petras, Failure mode maps for honeycomb sandwich panels, Compos. Struct. 44 (1999) 237–252. doi:http://dx.doi.org/10.1016/S0263-8223(98)00123-8.

[5] C. Chen, A.M. Harte, N.A. Fleck, Plastic collapse of sandwich beams with a metallic foam core, Int. J. Mech. Sci. 43 (2001) 1483–1506. doi:10.1016/S0020-7403(00)00069-2.

[6] F. Brenne, T. Niendorf, H.J. Maier, Additively manufactured cellular structures: Impact of microstructure and local strains on the monotonic cyclic behavior under uniaxial and bending load, J. Matierals Process. Technol. 213 (2013) 1558–1564.

[7] K.M. Conway, G.J. Pataky, Effective area method for calculating global properties of cellular materials, Mater. Today Commun. 17 (2018) 144–152. doi:10.1016/j.mtcomm.2018.09.003.

[8] K.M. Conway, S.S. Kulkarni, B.A. Smith, G.J. Pataky, G.M. Mocko, J.D. Summers, In-plane pure shear deformation of cellular materials with novel grip design, in: Solid Free. Fabr. 2019 Proc. 30th Annu. Int. Solid Free. Fabr. Symp., 2019: pp. 2296–2313.

[9] T.K. Pellinen, S. Xiao, S. Carpenter, E. Masad, H. Di Benedetto, R. Roque, Relationship between triaxial shear strength and indirect tensile strength of hot mix asphalt, J. Assoc. Asph. Paving Technol. 74 (2005) 347–379.

[10] D. Digilab, Dremel Digilab 3D45 Filament EcoABS, (2021) 1. https://digilab.dremel.com/service-3d45-filament-ecoabs (accessed April 29, 2021).

[11] P. Reu, Virtual strain gage size study, Exp. Tech. 39 (2015) 1–3. doi:10.1111/ext.12172.

[12] R.C. Hibbler, Theories of Failure, in: Mech. Mater., Eighth, Pearson Prentice Hall, Upper Saddle River, 2011: pp. 521–531.

[13] P. Köhnen, C. Haase, J. Bültmann, S. Ziegler, J.H. Schleifenbaum, W. Bleck, Mechanical properties and deformation behavior of additively manufactured lattice structures of stainless steel, Mater. Des. 145 (2018) 205–217. doi:10.1016/j.matdes.2018.02.062.

[14] M. Leary, M. Mazur, H. Williams, E. Yang, A. Alghamdi, B. Lozanovski, X. Zhang, D. Shidid, L. Farahbod-sternahl, G. Witt, I. Kelbassa, P. Choong, M. Qian, M. Brandt, Inconel 625 lattice structures manufactured by selective laser melting (SLM):

Mechanical properties , deformation and failure modes, Mater. Des. 157 (2018) 179–199. doi:10.1016/j.matdes.2018.06.010.

[15] T. Maconachie, M. Leary, B. Lozanovski, X. Zhang, M. Qian, O. Faruque, M. Brandt, SLM lattice structures: Properties, performance, applications and challenges, Mater. Des. 183 (2019) 1–18. doi:10.1016/j.matdes.2019.108137.

[16] X. Chen, Q. Ji, J. Wei, H. Tan, J. Yu, P. Zhang, V. Laude, M. Kadic, Light-weight shell-lattice metamaterials for mechanical shock absorption, Int. J. Mech. Sci. 169 (2020) 1–9. doi:10.1016/j.ijmecsci.2019.105288.

[17] L.J. Gibson, M.F. Ashby, Cellular Solids, structures and properties, 2nd ed., Cambridge University Press, Cambridge, 1997. doi:10.1016/S0304-0208(08)72856-1.

[18] K.M. Conway, G.J. Pataky, Crazing in additively manufactured acrylonitrile butadiene styrene, Eng. Fract. Mech. 211 (2019) 114–124. doi:10.1016/j.engfracmech.2019.02.020.

[19] Y. Sun, N.M. Pugno, In plane stiffness of multifunctional hierarchical honeycombs with negative Poisson ' s ratio sub-structures, Compos. Struct. 106 (2013) 681–689. doi:10.1016/j.compstruct.2013.05.008.

[20] C. Bonatti, D. Mohr, Large deformation response of additively-manufactured FCC metamaterials: From octet truss lattices towards continuous shell mesostructures, Int. J. Plast. 92 (2017) 122–147. doi:10.1016/j.ijplas.2017.02.003.

[21] Y. Boonyongmaneerat, D.C. Dunand, Effects of strut geometry and pore fraction on creep properties of cellular materials, Acta Mater. 57 (2009) 1373–1384. doi:10.1016/j.actamat.2008.11.027.

[22] C. Methods, A. Mech, A. Vigliotti, D. Pasini, Stiffness and strength of tridimensional periodic lattices, Comput. Methods Appl. Mech. Eng. 229–232 (2012) 27–43. doi:10.1016/j.cma.2012.03.018.